LANGMUIR

Interfaces: Adsorption, Reactions, Films, Forces, Measurement Techniques, Charge Transfer, Electrochemistry, Electrocatalysis, Energy Production and Storage

Ultra-flat Gold QCM Electrodes Fabricated with Pressure Forming Template Stripping for Protein Studies at the Nanoscale

Juan Antonio Rubio Lara, Frederik Bergler, Simon James Attwood, J. Michael Edwardson, and Mark E. Welland

Langmuir, **Just Accepted Manuscript** • DOI: 10.1021/acs.langmuir.8b03782 • Publication Date (Web): 12 Mar 2019

is published by the American Chemical Society. 1155 Sixteenth Street N.W., Washington, DC 20036

Ultra-flat Gold QCM Electrodes Fabricated with Pressure Forming Template Stripping for Protein Studies at the Nanoscale

Juan A. Rubio-Lara[†], Frederik Bergler [‡], Simon J. Attwood[†], J. Michael Edwardson [‡], Mark E. Welland*[,†]

[†]Nanoscience Centre, University of Cambridge. 11 JJ Thomson Ave, Cambridge CB3 0FF, United Kingdom.

[‡]Department of Pharmacology, University of Cambridge. Tennis Court Road, Cambridge, CB2 1PD, United Kingdom.

*Corresponding Author

KEYWORDS: atomically flat, gold, BSA, protein, monolayer, aggregation, roughness, electrodes, QCM, template, stripped, pressure, forming, AFM.

Abstract

Single-molecule imaging of proteins using atomic force microscopy (AFM) is crucially dependent on protein attachment to ultra-flat substrates. The technique of template stripping (TS), which can be used to create large areas of atomically flat gold, has been used to great effect for this purpose. However, this approach requires an epoxy which can swell in solution, causing surface roughening and substantially increasing the thickness of any sample, preventing its use on acoustic resonators in liquid. Diffusion bonding techniques should circumvent this problem but cannot be used on samples containing patterned features with mismatched heights due to cracking and poor transfer. Here, we describe a new technique called pressure forming template stripping (PTS) which permits an ultra-flat (0.35 ± 0.05 nm root-mean-square roughness) layer of gold to be transferred to the surface of a patterned substrate at low temperature and pressure. We demonstrate this technique by modifying a quartz crystal microbalance (QCM) sensor to contain an ultra-flat gold surface. Standard QCM chips have substantial roughness, preventing AFM imaging of proteins on the surface after measurement. With our approach there is no need to run samples in parallel: the modified QCM chip is flat enough to permit high-contrast AFM imaging after adsorption studies have been conducted. The PTS-QCM chips are then used to demonstrate adsorption of bovine serum albumin in comparison to rough QCM chips. The ability to attach thin layers of ultra-flat metals to surfaces of heterogeneous nature without epoxy will have many applications in diverse fields where there is a requirement to observe nanoscale phenomena with multiple techniques, including surface and interfacial science, optics, and biosensing.

Introduction

Atomically flat metallic surfaces have helped to improve protein characterization using atomic force microscopy (AFM), to increase enhancement of the plasmon effect for surface plasmon resonance (SPR) studies, to fabricate high-resolution flexible electronics, and to produce high quality lipid bilayers[1–4]. Until now, it was not possible to prepare these surfaces on specific areas of biosensors such as the electrodes of quartz crystal microbalance (QCM) resonators. One of the first techniques used to transfer an atomically flat surface to a target sample was introduced by Hegner et al, which they termed template-stripped gold (TSG)[5]. The method uses an epoxy glue to attach gold previously deposited on a mica template, onto a silicon wafer substrate. By removing the mica, the gold will have a flatness provided by the interface with the template. However, the spreading of the epoxy limits TSG to whole substrate samples. A similar method has been used for transferring mica onto QCM-D electrodes, but the yield is low (36%) due to the complexity of cleaving the mica from the resonator[6]. Two major drawbacks of using TSG prepared in this manner are the swelling of epoxy under organic and aqueous solvents, leading to roughening of the surface at the micron scale or tearing[7], and the fact that the resultant electrodes are typically 3-4 μm thicker than regular electrodes, which significantly affects the reliability of QCM measurements by inducing spurious responses[8]. To overcome the use of an epoxy, Blackstock et al[9] developed a technique called cold-welded template-stripped (CWTS), where deposited platinum on a silicon wafer template was coated with a gold film, which will bond to another gold film on the target substrate. The CWTS technique relies on compression to create diffusion bonding between the two gold films. The difficulties with this technique are that exposure to ambient conditions will stop the transfer, and that the use of plates to apply the pressure requires all substrates used to be of the exact same dimensions, otherwise the sample

will break. A variation of the CWTS technique, introduced by Mosley et al[10], uses gold on a mica template, which permits exposure to ambient conditions. By heating the sample during compression, the authors successfully transferred the templated gold under laboratory conditions. However, the method still requires samples to be of the same size, uses temperatures above 300°C, higher pressures than the CWTS method (240 bar) and a total gold thickness of 500 nm. Furthermore, the presence of holes on the surface limits its flatness over large areas. Nevertheless, it has been shown that cold welding of gold is possible under ambient conditions and low pressure by maximizing the contact between gold films using elastomeric templates[11]. Additionally, Lu et al demonstrated the cold welding of ultrathin gold nanowires by proximity contact[12], which supports the idea that low pressure can be used to bond two layers of gold by maximizing contact. Recently, Hugall et al showed that hardening liquid glass can be used as the target substrate having as an advantage the solvent resistant nature of this material[13]. However, the size and shape of the resultant surface is determined by the spreading of the glass droplet, which is poorly controlled, and compulsory use of this material makes the technique impractical for other substrates. Miller et al use chemical mechanical polishing (CMP) on gold-coated substrates that can be used for very large areas (44 cm^2) [14]. Their roughness values are in the same range as TSG samples: ~0.35 nm root-mean-square (RMS) over 1 μm^2 areas. The problems with CMP are: first, that it requires small steps between grain boundaries (5-6 nm) to keep a consistent small value of RMS roughness, which is possible only for very thin films (~50 nm)[15]; and second, the presence of residual iodine on the surface, which reduces the purity of the gold.

To overcome the issues of fabricating atomically flat surfaces on QCM resonators, we present the technique of pressure-forming template-stripping (PTS), which has the following advantages: i) compatibility with substrates containing laterally heterogeneous patterns of different materials,

ii) high reproducibility and yield, iii) variable thickness (≥80 nm) without affecting the flatness, iv) works on large-area samples (~1 cm^2), v) transfer of multiple samples at the same time, permitting high-throughput production, and vi) solvent resistance.

We apply the PTS technique to QCM resonators and observe how physical structures affect the adsorption of bovine serum albumin (BSA) by including the ideal scenario of an atomically flat surface. The interactions between BSA and the chemical composition of the surface have been studied before[16] and do not represent the objective of this work. The influence of surface roughness on BSA adsorption has also been studied by others[17,18]. The enhancement of adsorption of BSA to rough surfaces is attributed to both the denaturation of the protein at the surface and the increased surface area. These previous authors compared their measurements with standard samples (>1 nm RMS roughness over 1 μm^2). In principle, the elimination of nanostructures on QCM electrodes through the use of the PTS technique will decrease the amount of proteins adsorbed in comparison with a sample of standard roughness. We use PTS-QCM resonators and AFM in liquid to observe the areal mass density adsorption of BSA in the ideal case of a flat surface and compare it with standard QCM and rough QCM electrode surfaces.

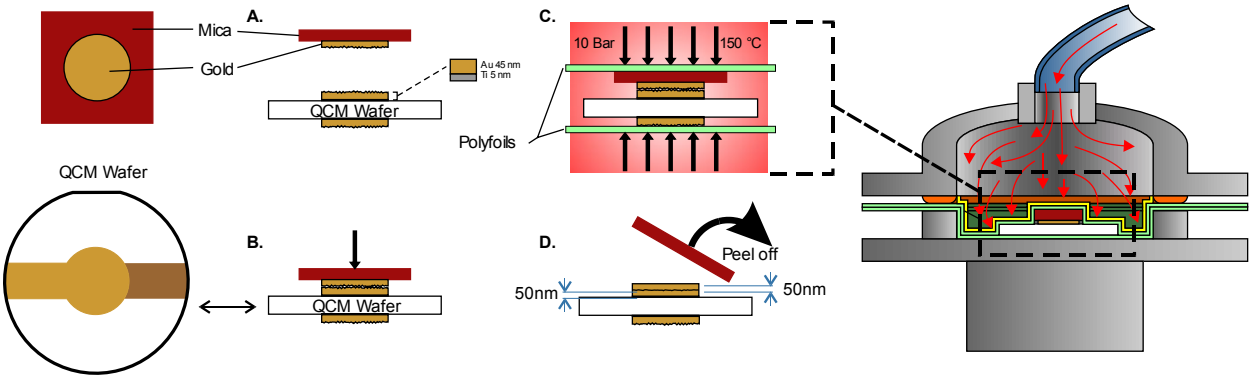

Figure 1. Pressure-forming template-stripping (PTS) of gold on a QCM resonator. (A) 50 nm of Au is evaporated on freshly-cleaved mica and (B) placed on top of a QCM wafer with a gold electrode of 50 nm total thickness. (C) A nanoimprinter that uses pressure forming, distributes pressurized air, represented by red arrows, on the sample using a polymer foil and thin mica substrates, increasing the contact of both gold surfaces. (D) Mica is mechanically cleaved to expose the atomically flat gold electrode.

EXPERIMENTAL SECTION

Materials and Methods. QCM resonators (9 MHz) for the standard roughness measurements were purchased from QuartzPro (Sweden). High fundamental frequency QCM (HFFQCM) of 50 MHz with standard electrode roughness and standard blank QCM resonators (10 MHz) were purchased from AWSensors S.L. (Paterna, Spain). QCM mass measurements were performed in the A20 research platform with an F20 fluidics module from AWSensors S.L., which directly outputs change of frequency and dissipation of the adsorbed layer. Ruby muscovite mica squares with 11 mm sides and 0.15 mm thickness were purchased from Agar Scientific Ltd, (UK).

Evaporations were performed on a PVD 75 Kurt J. Lesker e-beam evaporator for Ti and Au on target samples. Thermal evaporation of Au on mica was carried out on a BOC Edwards Auto 306 resistance evaporator. Shadow masks were purchased from Laser Micromachining Limited (UK). Pure gold, 99.99%, in pieces of 3 mm was purchased from Kurt J. Lesker (UK). UV ozone treatment was applied using the ProCleaner (BioForce Nanosciences) for 25 min.

AFM images in air were taken using Veeco Enviroscope with Nanosensors SSS-NCH tips (radius of curvature <5 nm) from Windsor Scientific (UK), and images in liquid were taken using the Bruker FastScan with FastScan-D tips (<8 nm) from Bruker (France). All measurements were obtained in tapping mode. The pressure-forming technique was performed in

a NIL 2.5 Obducat Nanoimprinter with programmable temperature and pressure controller using poly-foils (imprint membranes) of 100 mm diameter from Obducat (Sweden). BSA ≥98% was purchased from Sigma Aldrich (UK) and dissolved in Sörensen's buffer at a pH of 7.4 (see supporting information). High-performance liquid chromatography (HPLC) grade water was purchased from Fisher Scientific (UK) and freshly used.

Fabrication of Pressure-Forming Template-Stripping (PTS) of Gold. The fabrication of PTS gold is outlined in Figure 1. Blank QCM crystals of 10 MHz were coated with 5 nm of titanium as an adhesion layer, with 95 nm of gold on top for the back electrode, and 45 nm of gold for the target electrode. A total of 100 nm-thick electrodes is the standard for QCM resonators to avoid inducing inharmonic modes and affecting the measurement[19,20]. Cr should be avoided as this might contaminate the gold when the temperature is increased[21]. Fifty nanometers of gold was thermally evaporated onto freshly-cleaved mica (<100 μm thick) through a shadow mask at 4 nm/s, which resulted in larger grains essential for PTS, as compared to lower rates (see Figure S1). The mask is not required on the template, see Figure S2, but it was used for quick alignment and to obtain the same area transferred consistently. The gold on mica was placed in contact with the target gold electrode of the QCM, leaving the mica on top of the stack. One poly-foil was placed below and another above the combined substrates. Using a technique resembling pressure forming, heat and pressure was applied to the poly-foil on top of the mica using a Nanoimprinter. The thin, flexible mica sheet in combination with the poly-foil permits conformal contact of both gold layers with even pressure distribution, which reduces the total pressure required and reduces the time over which the transfer occurs successfully[11]. The temperature was increased to 150°C for 1000 s, followed by cooling to 50°C and heating again to 150°C for 120 s. The sample was finally cooled to 50°C. The two-step heating at 150°C resulted

in larger grains than a one-step heating for the same time. The transfer was performed at a constant pressure of 10 bar and took 40 min to complete. Finally, and immediately prior to experiment, the mica was mechanically stripped from the QCM resonator, leaving an atomically flat gold surface (see Figure 2A). Because of the low pressure and the way pressure forming distributes the load using poly-foils, the mismatch between the mica and the QCM resonator does not damage the sample. Using a hard substrate such as silicon would, for example, crack the QCM chip as well as leading to only partial transfer (see Figure S2). This method was not tested on target substrates thicker than the standard silicon wafer (~512 μm), and it might not work for thicknesses beyond this because of the maximum deformation possible of the poly-foils. The resulting QCM resonator with PTS gold (PTS-QCM) can be stored for months before the stripping is performed.

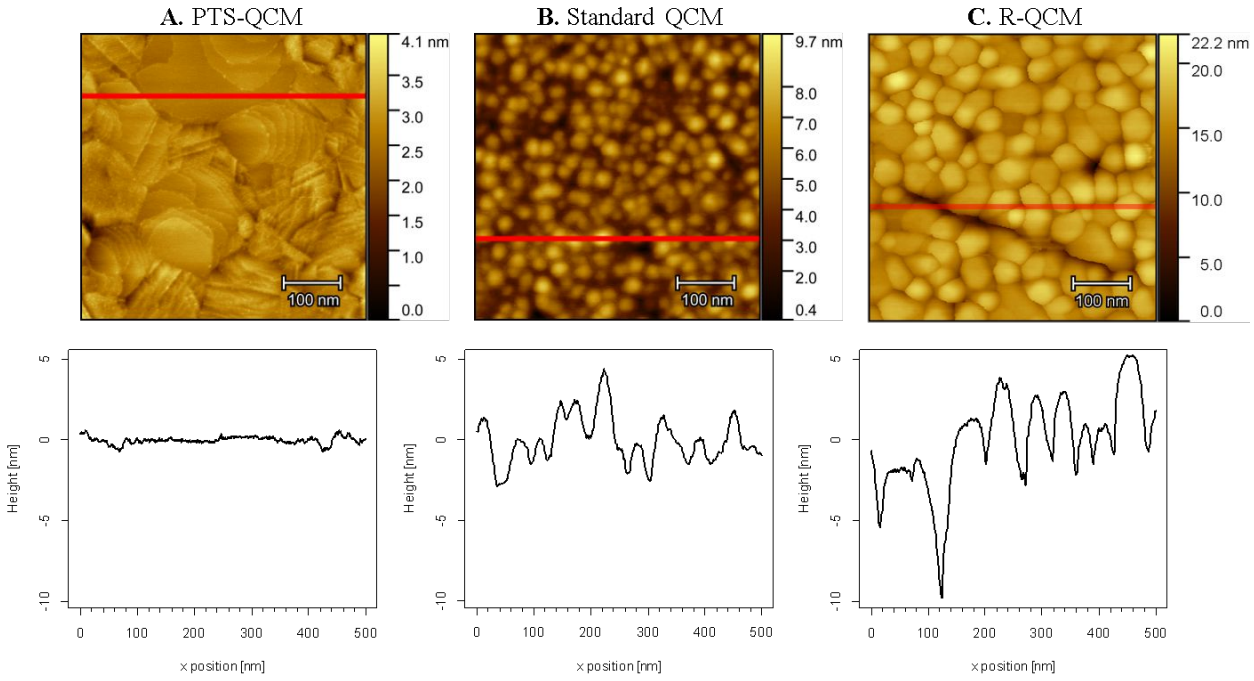

Figure 2. Comparison of roughness observed on three gold-coated QCM resonators, measured with AFM. (A) Ultra-flat gold prepared using the PTS technique; (B) Standard QCM chip

without modification; (C) Rough QCM (R-QCM) fabricated in-house. Below are corresponding height profiles. Images are 500 nm square.

Fabrication of QCM with Rough Electrodes. QCM with rough gold electrodes (R-QCM) were fabricated in-house by e-beam evaporation of 5 nm of Ti (at 0.5Å/s) and 95 nm of Au (1Å/s) on both sides of the crystal at $1x10^{-6}$ Torr, see Figure 2C.

Results and Discussion

PTS-QCM Resonators. The RMS roughness of PTS has an average value of 0.35 ± 0.05 nm (see Table S1) with comparable flatness reported for other methods:0.28± 0.01[5], 0.2-0.5[10], 0.275[13], and 0.21 nm RMS[22]. Grains are estimated to have a diameter of 200-500 nm, as it is difficult to detect grain boundaries accurately. In some cases, grains were bigger than the imaged areas (1 μm^2), see Figure S3. A cross-section image of the transfer can be seen in Figure S4. Pinholes are a well-known problem in template stripped techniques using gold[5,10,23], and were present on the surface of PTS gold prepared using evaporation rates <0.5 nm/s and thick gold films on mica (100-400 nm), as can be seen in Figure S1. It is believed that high rates of evaporation reduce the drag of contamination during the deposition as well as reducing the roughness of the exposed surface of the gold on mica. The contamination will limit the size of the grain, favoring the bonding of grains vertically (across gold films) but not laterally (on the same film). Therefore, high roughness on the exposed surface of the templated gold and contamination (e.g. thick film and low rate of evaporation, respectively) will increase the release of energy at the interface with mica during the bonding, leaving a hole as a result on the expected flat surface. High rates of 4 nm/s favor both vertical diffusion (transfer) and lateral coalescence (grain area increase) irrespective of thickness, eliminating the appearance of pinholes (see Figure S1). Rates higher than 4 nm/s did not improve the quality of the surface, and control of the

thickness was difficult to achieve, therefore, these rates were not used in our final results. The flat gold film of PTS should be flat and contamination free but there might be traces of Si and Al as a result of the stripping of mica[7].

BSA Mass Adsorption. After fabrication, PTS-QCM resonators (n=4) were used to adsorb a monolayer of BSA monomers (spherical model with ~7 nm diameter[24]) and their appearance compared with a QCM chip with standard roughness from QuartzPro (n=2), an HFFQCM resonator with standard roughness from AWSensors (n=1), and a R-QCM resonator with rough electrodes (n=2). All resonators were UV/ozone treated to remove any carbonaceous deposition[25] before they were installed on the QCM platform. AFM images of the electrodes of the QCM resonators used in this experiment are shown in Figure S5. Samples were left to stabilize under HPLC water for at least 16 h as well as to remove any oxide from the gold created by the UV/ozone treatment[26]. Buffer was run through all resonators for a couple of hours before one milliliter of BSA solution (100 μM) was injected onto all resonators at 50 μl/min.

Table 1. Summary of BSA adsorption to gold with different surface roughness and their characteristics[a].

Sample	Roughness RMS [nm]	Grains	Mass Adsorbed	$\lvert\Delta D_n/(\Delta f_n/n)\rvert$ [$1x10^{-8}Hz^{-1}$]	Coverage
		Diameter [nm]	Areal Mass Density [ng/cm^2]		
Regular Roughness (QuartzPro)	1.25	28 ±8	697 ±3	2.07 ±0.21	monolayer
Regular Roughness (AWSensors)	0.94	46 ±15	701	0.32	monolayer
Rough (R-QCM)	2.01	47 ±12	817 ±3	1.94 ±0.10	>monolayer
Ultra-Flat (PTS-QCM)	0.35	--	802 ±22	1.97 ±0.10	monolayer

[a]Four QCM chips with surfaces of regular roughness (QuartzPro, AWSensors), extra-rough surface (R-QCM) and an ultra-flat surface prepared with the PTS technique (PTS-QCM). Roughness and grain diameters of bare chips were determined using AFM. Adsorbed areal mass of BSA was determined using the QCM.

The areal mass densities of BSA adsorbed by each resonator are summarized in Table 1 using the Sauerbrey equation[27] (see Supporting Information) and curves of the change of frequency experiment due to areal mass adsorption along with its change of dissipation can be seen in Figure 3. Fundamental frequency and the next two harmonics were used to calculate the mass on all resonators with the exception of the HFFQCM where only the fundamental mode was used (50MHz). The protein coating was assumed to be rigid as all results for dissipation fulfill the relationship $|\Delta D_n/(\Delta f_n/n)| << 2.2 \times 10^{-7}$ for f_n=9MHz, $|\Delta D_n/(\Delta f_n/n)| << 2 \times 10^{-7}$ for f_n=10MHz, and $|\Delta D_n/(\Delta f_n/n)| << 4 \times 10^{-8}$ for f_n=50MHz, as well as having similar values between them[28]. The control samples with standard surface roughness (~1 nm RMS; QuartzPro and AWSensors) show the adsorption of a monolayer of BSA with an average of 697±3 ng/cm^2 of mass. The PTS-QCM resonator adsorbed 802±22 ng/cm^2, a 14.8% increase over control samples. Additionally, the rough sample, labelled Rough (R-QCM), showed an unexpected increase of 17.0% compared to control samples, when the expected area increase due to the increased topography measured by AFM is only 4.5% (surface area measured by AFM of R-QCM electrode divided by the surface area of QuartzPro sample).

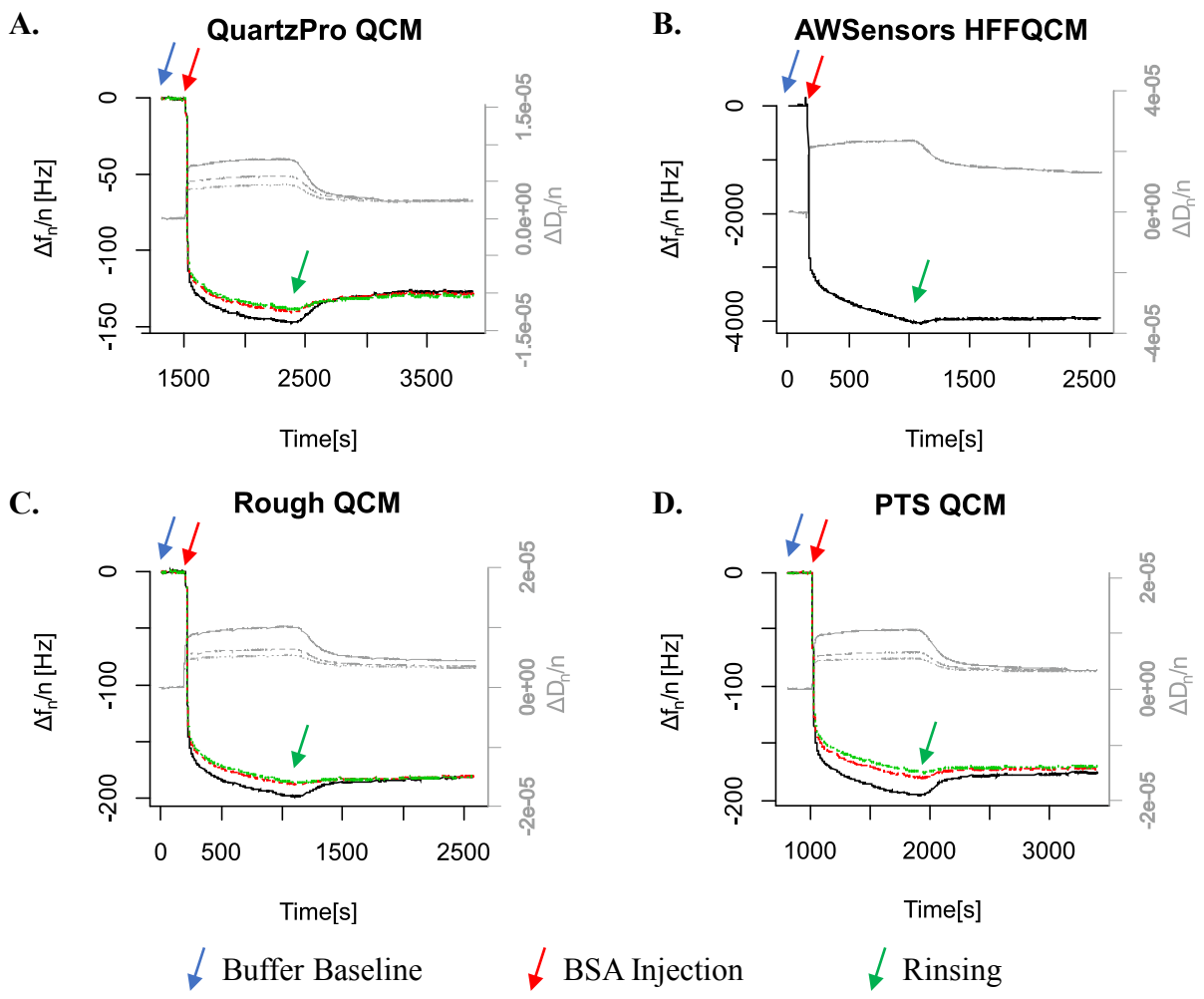

Figure 3. Bovine serum albumin adsorption on different gold surfaces. Standard gold roughness is found in samples (A) and (B), rough gold in (C) and atomically flat gold using pressure template stripping in (d). Black curve is the fundamental frequency, red curve the third harmonic, and green curve the fifth harmonic mode. For HFFQCM only the fundamental mode was obtained. The change of dissipation (ΔD) is plotted as gray curves for all harmonic responses in all resonators (right y axis). All samples were in buffer before injecting the protein (blue arrows), BSA solution was injected after three minutes in these plots (red arrows), the solution was changed back to buffer after 20 minutes (green arrows). All resonators have electrodes of 100 nm thickness.

AFM Imaging in Liquid. To observe the behavior of adsorbed BSA on the surfaces with increased mass (PTS-QCM and the R-QCM), samples were kept in buffer and AFM images were promptly taken (see Figure 4). To keep the sample in buffer, the QCM resonators were removed from the microfluidic chamber by carefully keeping the crystal horizontally and hence the buffer droplet on top, it was then transferred to an AFM disc with double sided tape. Results show that the high contrast provided by the PTS-QCM permits the visualization of a monolayer of BSA on this surface. This is corroborated by the absence of isolated BSA monomers on the image, see Figure S6. Rather, groups of proteins with a 7-nm periodicity were seen (see profile 1 in Figure 4A and Figure S6B, S6D). The contrast shown by the R-QCM samples, on the other hand, was poor, complicating the analysis due to the nanoscale roughness. Nevertheless, features of 20-30 nm in size (monomers adsorbing on top of another layer, plus a contribution due to the finite size of the tip) were observed, in agreement with other findings[29], and indicating monomer aggregates on top of the monolayer (see profile 1 in Figure 4B and model in Figure S6E and S6F). A monolayer was detected under the isolated monomers, as can be seen in profile 2 of Figure 4B and Figure S6F. Multilayer BSA due to denaturation is expected for hydrophobic surfaces[30–34]. However, in the case of R-QCM samples, it is the roughness and grain dimensions that induce denaturation and hence BSA aggregation, as previously observed by others[18,35,36]. For comparison, an induced layer with aggregates of BSA on hydrophobic PTS-QCM is shown in Figure S7 (equivalent to model in Figure S6F), which demonstrates the high contrast of PTS required to characterize monomer aggregation studies quantitively.

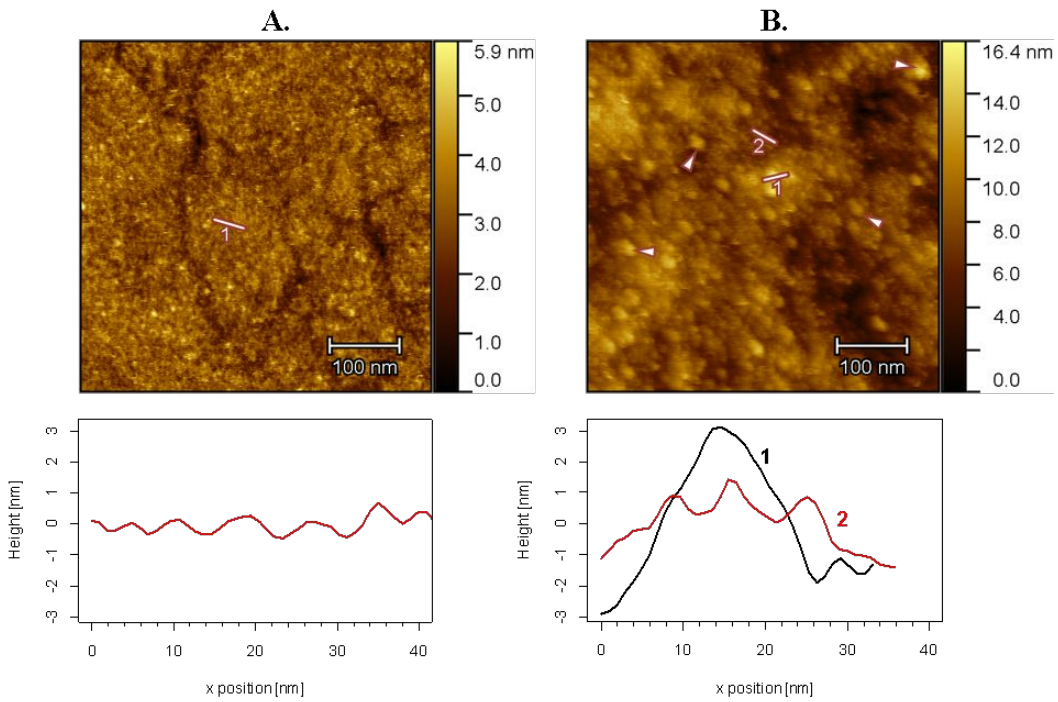

Figure 4. AFM topography images recorded in PBS for BSA adsorbed to (A) ultra-flat gold PTS-QCM samples, and (B) rough gold R-QCM samples. Monolayer adsorption is observed in profile 1 (red) of (A) with features of 7 nm periodicity and steps of <2 nm (possibly from domains I and III[37]). The presence of isolated globules of 20-30 nm diameter in profile 1 (black) of (B) are BSA monomers adsorbed on top of another continuous layer as seen in profile 2 (red) of (B) (with 7-8 nm periodicity and steps of <2 nm) proving the presence of aggregates. Arrows in (B) point to some of the many isolated BSA monomers on top of a monolayer.

BSA Denatures due to Curvatures at the Nanoscale. The adsorption of BSA upon binding has been described as protein spreading in a molten-globule-like state[38,39]. The higher the concentration and saturation of the surface, the less likely the protein is to be able to rearrange to cover the empty areas. Thus, lower concentrations will induce protein spreading and higher concentrations will minimize it. In all our experiments the BSA has a concentration of 100 μM,

higher than the 50 μM required for a monolayer on standard QCM resonators (data not shown). For standard resonators, we believe that BSA molecules adsorb at different angles, depending on the region in which they landed on a grain and the radius of curvature, see models in Figure S8. Different angles of the adsorbed proteins will create steric effects for the next abutting protein, and so forth, eventually leading to the generation of an intermittent monolayer during saturation, with the possibility of subsequent spreading of the BSA minimizing surface energy. The standard QCM resonator leads to the smallest attached mass of all the conditions tested, as depicted on Figure S8C and S8D. We believe that the increase of mass in atomically flat electrodes is caused by proteins binding at normal angles to the grains, analog to binding to a perfect flat gold surface without grains or boundaries, reducing steric effects for the next neighboring protein, allowing more proteins to bind per area and creating a tightly packed monolayer, as can be seen in Figure 4A and Figure S8B. Grain boundaries might also play a role, as there are fewer grains on PTS-QCM than on rough surfaces and standard samples. In rough samples, a monolayer with the same characteristics as the standard roughness is obtained. Additionally, we believe that bigger steps on the boundaries and larger radii of curvature of the grains induce denaturation of some BSA monomers, see Figure S8E. This denaturation exposes inner groups in the protein that will induce a subsequent BSA molecule to bind, causing aggregation[40]. This agrees with the observed multilayer formation of BSA due to denaturation on prolonged adsorption on mica[41]. It is possible that the protrusions observed in the arrows of Figure 4B are a result of the roughness of the gold underlayer, which we believe is unlikely as Figure 2C does not present protrusions of this small scale (26 nm width, 6 nm height). These observations lead us to the following model: at zero roughness, the BSA is orderly packed in a monolayer; at a certain value of low roughness the BSA orientation is affected and binds disorderly creating a monolayer with less mass

adsorbed than the zero roughness case; at a higher roughness, more mass is adsorbed than in the low roughness case due to more area being available for the protein to bind, and additionally the features on the grains denatures some proteins on the monolayer inducing a second non-assembled layer on top.

Summary and Conclusions

Here, we present the fabrication of atomically flat gold electrodes on QCM resonators using the PTS technique, achieving 0.35 ± 0.05 nm RMS roughness. The method uses low pressure and temperature (10 bar and 150°C), allowing its use on substrates with multistep materials such as a quartz crystal with a deposited electrode. The direct transfer of the templated gold without using epoxies makes it solvent resistant and permits the fabrication of thin QCM electrodes without affecting the multiple-harmonics response to mass adsorption or inducing spurious responses caused by thick electrodes. Furthermore, our characterization of the resulting surface showed qualitatively that high rates of evaporation enhance the flatness by increasing the grain size of the film and reducing the number of pinholes present.

We further used the PTS-QCM resonator for BSA adsorption and showed that the protein adsorbs in a tightly-packed monolayer on atomically flat gold surfaces. This result was compared with the behavior of standard and rough QCM gold electrodes. In the rough QCM resonator, more mass was adsorbed than on the standard QCM by aggregation caused by the grain characteristics of the surface. We showed by AFM that a monolayer was present on some areas of the rough surface, which we believe to be on flat areas of grains, and that aggregates were induced, possibly, on grain edges and boundaries. The PTS-QCM showed more mass adsorbed compared to standard QCM, and AFM measurements in liquid proved that a tightly packed monolayer was the reason for this enhancement, i.e. more mass is adsorbed per area. This result

runs counter to the idea that rougher electrodes adsorb more mass. Instead, it is the grain boundaries and radius of curvature of the features on the surface that cause different distributions of charge that will make BSA bind at different angles, eventually inducing more mass adsorption due to formation of aggregates caused by denaturation at higher roughness.

The featureless PTS-QCM would allow studies of proteins in combination with other surface characterization techniques, as shown in this work using AFM. Its high contrast would benefit the observation of phenomena using the same sample. PTS should find important uses in areas including electrochemistry, surface science, lipid membrane studies, and nanoscale optics.

Associated Content

Supporting Information.

Roughness dependence of rate of evaporation and thickness for PTS gold; photographs of PTS of gold used on QCM resonators; AFM image of second PTS gold sample; SEM cross-sectional image of PTS on a silicon wafer; surface roughness of the electrodes used for the protein adsorption experiment; AFM profile models of proteins adsorbed as monolayer and multilayers; multilayer BSA on PTS gold; two-dimensional model of BSA adsorption on surfaces; roughness measurements of PTS-QCM electrodes; Sauerbrey Equation; Sörensen's phosphate buffer.

Author Information

*Mark E. Welland: Nanoscience Centre, University of Cambridge. 11 JJ Thomson Ave, Cambridge CB3 0FF, United Kingdom.

Present Addresses

†Juan A. Rubio-Lara: School of Clinical Medicine, University of Cambridge. Clifford Allbutt Building, Hills Road, Room 518, Cambridge Biomedical Campus, Cambridge, CB2 0AH.

Author Contributions

The manuscript was written through contributions of all authors. All authors have given approval to the final version of the manuscript.

Acknowledgment

JRL would like to acknowledge the Cambridge Trust, CONACyT (Mexico) and Secretaría de Educación Pública (SEP, Mexico) for his PhD Scholarship. JRL also acknowledges the funding support of the University of Cambridge Student Registry and Fitzwilliam College, Cambridge.

References

(1) Attwood, S. J.; Simpson, A. M. C.; Stone, R.; Hamaia, S. W.; Roy, D.; Farndale, R. W.; Ouberai, M.; Welland, M. E. A Simple Bioconjugate Attachment Protocol for Use in Single Molecule Force Spectroscopy Experiments Based on Mixed Self-Assembled Monolayers. *Int. J. Mol. Sci.* **2012**, *13* (10), 13521–13541.

(2) De Nijs, B.; Benz, F.; Barrow, S. J.; Sigle, D. O.; Chikkaraddy, R.; Palma, A.; Carnegie, C.; Kamp, M.; Sundararaman, R.; Narang, P.; et al. Plasmonic Tunnel Junctions for Single-Molecule Redox Chemistry. *Nat. Commun.* **2017**, *8* (1), 1–8.

(3) Tan, E. K. W.; Rughoobur, G.; Rubio-lara, J.; Tiwale, N.; Xiao, Z.; Davidson, C. A. B.; Lowe, C. R.; Occhipinti, L. G. Nanofabrication of Conductive Metallic Structures on Elastomeric Materials. *Sci. Rep.* **2018**, 1–9.

(4) Knoll, W.; Köper, I.; Naumann, R.; Sinner, E. K. Tethered Bimolecular Lipid Membranes-A Novel Model Membrane Platform. *Electrochim. Acta* **2008**, *53* (23), 6680–6689.

(5) Hegner, M.; Wagner, P.; Semenza, G. Ultralarge Atomically Flat Template-Stripped Au Surfaces for Scanning Probe Microscopy. *Surf. Sci.* **1993**, *291* (1–2), 39–46.

(6) Richter, R. P.; Brisson, A. QCM-D on Mica for Parallel QCM-D-AFM Studies. *Langmuir* **2004**, *20* (11), 4609–4613.

(7) Wagner, P.; Hegner, M.; Güntherodt, H. J.; Semenza, G. Formation and in Situ Modification of Monolayers Chemisorbed on Ultraflat Template-Stripped Gold Surfaces. *Langmuir* **1995**.

(8) Shockley, W.; Koneval, D. J. Trapped-Energy Modes in Quartz Filter Crystals. *J. Acoust. Soc. Am.* **1966**, *268* (April 1965), 981–993.

(9) Blackstock, J. J.; Li, Z.; Jung, G. Template Stripping Using Cold Welding. *J. Vac. Sci. Technol. A Vacuum, Surfaces, Film.* **2004**, *22* (3), 602.

(10) Mosley, D. W.; Chow, B. Y.; Jacobson, J. M. Solid-State Bonding Technique for Template-Stripped Ultraflat Gold Substrates. *Langmuir* **2006**, *22* (6), 2437–2440.

(11) Ferguson, G. S.; Chaudhury, M. K.; Sigal, G. B.; Whitesides, G. M. Contact Adhesion of Thin Gold Films on Elastomeric Supports: Cold Welding under Ambient Conditions. *Science (80-.).* **1991**, *253* (5021), 776–778.

(12) Lu, Y.; Huang, J. Y.; Wang, C.; Sun, S.; Lou, J. Cold Welding of Ultrathin Gold Nanowires. *Nat. Nanotechnol.* **2010**, *5* (3), 218–224.

(13) Hugall, J. T.; Finnemore, A. S.; Baumberg, J. J.; Steiner, U.; Mahajan, S. Solvent-Resistant Ultraflat Gold Using Liquid Glass. *Langmuir* **2012**, *28* (2), 1347–1350.

(14) Miller, M. S.; Ferrato, M.; Niec, A.; Biesinger, M. C.; Carmichael, T. B. Ultrasmooth Gold Surfaces Prepared by Chemical Mechanical Polishing for Applications in Nanoscience. *Langmuir* **2014**, *30* (47), 14171–14178.

(15) Petrov, I.; Barna, P. B.; Hultman, L.; Greene, J. E. Microstructural Evolution during Film Growth. *J. Vac. Sci. Technol. A Vacuum, Surfaces, Film.* **2003**, *21* (5), S117.

(16) Roach, P.; Farrar, D.; Perry, C. C. Surface Tailoring for Controlled Protein Adsorption: Effect of Topography at the Nanometer Scale and Chemistry. *J. Am. Chem. Soc.* **2006**, *128* (12), 3939–3945.

(17) Dolatshahi-Pirouz, A.; Rechendorff, K.; Hovgaard, M. B.; Foss, M.; Chevallier, J.; Besenbacher, F. Bovine Serum Albumin Adsorption on Nano-Rough Platinum Surfaces Studied by QCM-D. *Colloids Surf. B. Biointerfaces* **2008**, *66* (1), 53–59.

(18) Rechendorff, K.; Hovgaard, M. B.; Foss, M.; Zhdanov, V. P.; Besenbacher, F. Enhancement of Protein Adsorption Induced by Surface Roughness. *Langmuir* **2006**, *22* (26), 10885–10888.

(19) Curran, D. R.; Koneval, D. J. Factors in the Design of VHF Filter Crystals. In *19th Annual Symposium on Frequency Control*; 1965; pp 213–268.

(20) Shockley, W.; Curran, D. R.; Koneval, D. J. Trapped-Energy Modes in Quartz Filter Crystals. *J. Acoust. Soc. Am.* **1967**, *41* (4B), 981–993.

(21) Huang, Y.; Qiu, H.; Wang, F.; Pan, L.; Tian, Y.; Wu, P. Effect of Annealing on the Characteristics of Au/Cr Bilayer Films Grown on Glass. *User Model. User-adapt. Interact.* **2003**, *71* (4), 523–528.

(22) DeRose, J. A.; Thundat, T.; Nagahara, L. A.; Lindsay, S. M. Gold Grown Epitaxially on Mica: Conditions for Large Area Flat Faces. *Surf. Sci.* **1991**, *256* (1–2), 102–108.

(23) Banner, L. T.; Richter, A.; Pinkhassik, E. Pinhole-Free Large-Grained Atomically Smooth Au(111) Substrates Prepared by Flame-Annealed Template Stripping. *Surf. Interface Anal.* **2009**, *41* (1), 49–55.

(24) Axelsson, I. Characterization of Proteins and Other Macromolecules by Agarose Gel Chromatography. *J. Chromatogr. A* **1978**.

(25) Bolon, D. A.; Kunz, C. O. Ultraviolet Depolymerization of Photoresist Polymers. *Polym. Eng. Sci.* **1972**, *12* (2), 109–111.

(26) Krozer, A.; Rodahl, M. X-Ray Photoemission Spectroscopy Study of UV/Ozone Oxidation of Au under Ultrahigh Vacuum Conditions. *J. Vac. Sci. Technol. A Vacuum, Surfaces, Film.* **1997**, *15* (3), 1704–1709.

(27) Sauerbrey, G. Verwendung von Schwingquarzen Zur Wägung Dünner Schichten Und Zur Mikrowägung. *Zeitschrift für Phys.* **1959**, *155* (2), 206–222.

(28) Reviakine, I.; Johannsmann, D.; Richter, R. P. Hearing What You Cannot See and Visualizing What You Hear. *Anal. Chem.* **2011**, *83*, 8838–8848.

(29) Quist, a P.; Bjorck, L. P.; Reimann, C. T.; Oscarsson, S. O.; Sundqvist, B. U. R. A Scanning Force Microscopy Study of Human Serum-Albumin and Porcine Pancreas Trypsin Adsorption on Mica Surfaces. *Surf. Sci.* **1995**, *325* (1–2), L406–L412.

(30) Ouberai, M. M.; Xu, K.; Welland, M. E. Effect of the Interplay between Protein and Surface on the Properties of Adsorbed Protein Layers. *Biomaterials* **2014**, *35* (24), 6157–6163.

(31) Wehmeyer, J. L.; Synowicki, R.; Bizios, R.; García, C. D. Dynamic Adsorption of Albumin on Nanostructured TiO2 Thin Films. *Mater. Sci. Eng. C* **2010**, *30* (2), 277–282.

(32) Guo, S.; Pranantyo, D.; Kang, E. T.; Loh, X. J.; Zhu, X.; Jańczewski, D.; Neoh, K. G. Dominant Albumin-Surface Interactions under Independent Control of Surface Charge and Wettability. *Langmuir* **2018**, *34* (5), 1953–1966.

(33) Sakata, S.; Inoue, Y.; Ishihara, K. Molecular Interaction Forces Generated during Protein Adsorption to Well-Defined Polymer Brush Surfaces. *Langmuir* **2015**, *31* (10), 3108–3114.

(34) Roach, P.; Farrar, D.; Perry, C. C. Interpretation of Protein Adsorption: Surface-Induced Conformational Changes. *J. Am. Chem. Soc.* **2005**, *127* (22), 8168–8173.

(35) Dolatshahi-Pirouz, a; Rechendorff, K.; Hovgaard, M. B.; Foss, M.; Chevallier, J.; Besenbacher, F. Bovine Serum Albumin Adsorption on Nano-Rough Platinum Surfaces Studied by QCM-D. *Colloids Surf. B. Biointerfaces* **2008**, *66* (1), 53–59.

(36) Riedel, M.; Müller, B.; Wintermantel, E. Protein Adsorption and Monocyte Activation on Germanium Nanopyramids. *Biomaterials* **2001**, *22* (16), 2307–2316.

(37) Bujacz, A. Structures of Bovine, Equine and Leporine Serum Albumin. *Acta Crystallogr.*

Sect. D Biol. Crystallogr. **2012**, *68* (10), 1278–1289.

(38) Ptitsyn, O. How Molten Is the Molten Globule? *Nat. Struct. Biol.* **1996**, *3* (6), 488–490.

(39) Dolgikh, D. A.; Gilmanshin, R. I.; Brazhnikov, E. V.; Bychkova, V. E.; Semisotnov, G. V.; Venyaminov, S. Y.; Ptitsyn, O. B. A-Lactalbumin: Compact State With Fluctuating Tertiary Structure? *FEBS Lett.* **1981**, *136* (2), 311–315.

(40) Bhattacharya, M.; Jain, N.; Mukhopadhyay, S. Insights into the Mechanism of Aggregation and Fibril Formation from Bovine Serum Albumin. *J. Phys. Chem. B* **2011**, *115* (14), 4195–4205.

(41) Terashima, H.; Tsuji, T. Adsorption of Bovine Serum Albumin onto Mica Surfaces Studied by a Direct Weighing Technique. *Colloids Surfaces B Biointerfaces* **2003**, *27* (3/2), 115–122.

TOC